COMPRESSIBLE UNSTEADY AERODYNAMICS FOR AEROELASTIC ANALYSIS OF HELICOPTER BLADES WITH TRAILING EDGE FLAPS AND ITS IMPLEMENTATION

Timothy F. Myrtle*and Peretz P. Friedmann†
Mechanical and Aerospace Engineering Department
University of California, Los Angeles
Los Angeles, California USA

Abstract

This paper describes a new, two-dimensional, compressible unsteady aerodynamic model developed for dynamic analysis of a rotor blade/actively controlled flap combination. Aerodynamic loads are approximated in the frequency domain as rational functions of the Laplace variable using a least squares fit to oscillatory response data. Transformation to the time domain yields a state space model for the unsteady aerodynamic loads. Expressions for the unsteady lift, moment, and hinge moment for an airfoil/flap combination are presented. Frequency domain loads are obtained using a two dimensional doublet-lattice analysis. A provision is included for representing the unsteady effects associated with time-varying freestream. The aerodynamic model for the airfoil/flap is implemented in an aeroelastic simulation of a fully elastic hingeless helicopter rotor with a partial span trailing edge flap. A time domain solution of the coupled trim/aeroelastic response problem is presented together with illustrative results.

List of Symbols

b	Blade semi-chord,
c_b	Blade chord
C_{do}	Blade drag coefficient
C_h	Sectional hinge moment coefficient
C_l	Sectional lift coefficient
C_m	Sectional moment coefficient
C_W	Weight coefficient, $C_W = \frac{Weight}{\pi R^2 \rho_A R^2 \Omega^2}$
D_0	Generalized flap motion producing constant normal velocity distribution on flap
D_1	Generalized flap motion producing linearly varying normal velocity distribution on flap
fC_{df}	Equivalent fuselage flat plate area
$F(\mathbf{x}_{dv})$	Objective function
$F(k_n)$	Real part of nth oscillatory data point
$G(k_n)$	Imaginary part of nth oscillatory data point
$g(\mathbf{x}_{dv})$	Constraint equation
h	Plunge displacement of 1/4 chord
k	Reduced freq, $\omega b/U_o$
L_b	Length of blade
M	Mach number
M_b	Mass of one blade
N_b	Number of blades
N_c	Number of constraint equations
N_{dp}	Number of oscillatory data points
N_{dv}	Number of design variables
N_p	Number of lag terms
p	Laplace variable
$\tilde{p}$	Nondim. Laplace variable, $\tilde{p} = \frac{pb}{U_o}$
$\mathbf{q_b}$	Blade degrees of freedom
$\mathbf{q_t}$	Trim parameters
$Q(\tilde{p})$	Transfer function relating generalized motion to aerodynamic load
R	Rotor radius
$\mathbf{R}$	Vector of trim equation residuals
t	Time
$[T_o]$	Matrix of control sensitivities
s	Nondim. time, $s = \frac{1}{b}\int_0^t U(\tau)d\tau$
U	Freestream velocity
U_o	Constant portion of freestream velocity
V_F	Helicopter forward flight velocity
W_0	Generalized airfoil motion producing constant normal velocity distribution on chord
W_1	Generalized airfoil motion producing linearly varying normal velocity distribution on chord
x_j, z_n	Aerodynamic state variables
$\mathbf{x_a}$	Aerodynamic states
x_{dvi}	ith design variable
$\mathbf{x}_{dv}$	Vector of design variables
x_{Ui}, x_{Li}	Upper and lower limits on the ith design variable
X_{FA}	Horizontal offset of fuselage aerodynamic center from hub
X_{FC}	Horizontal offset of fuselage center of gravity from hub
Z_{FA}	Vertical offset of fuselage aerodynamic center from hub
Z_{FC}	Vertical offset of fuselage center of gravity from hub
α	Angle between chordline and freestream
α_o	Constant portion of α
α_R	Rotor angle of attack

*Ph.D. Candidate
†Professor

γ_j	Rational approximant pole
γ	Lock Number
δ	Flap deflection angle
ϵ	Dimensionless parameter representative of blade slope
θ_{pt}	Blade pretwist distribution
$\theta_0, \theta_{1c}, \theta_{1s}$	Collective and cyclic pitch components
κ_j	Rational approximant pole
λ	Error weighting parameter
λ_u	Nondim. freestream velocity amplitude $(\Delta U/U_o)$
μ	Advance ratio, $\frac{V_F \cos\alpha_R}{\Omega R}$
ρ_A	Air density
σ	Blade solidity ratio
$\mathcal{X}$	Least square error parameter
ψ	Blade azimuth angle, $\psi = \Omega t$
ω	Frequency
ω_F	Rotating flap frequency
ω_L	Rotating lead-lag frequency
ω_T	Rotating torsional frequency
Ω	Rotor angular speed
$\dot{()}$	$d()/dt$
$\mathcal{L}[]$	Laplace operator

Introduction

Vibration is a problem of major concern for helicopter manufacturers due to its impact on helicopter comfort, performance, and reliability. With military and civilian customers adopting increasingly stringent requirements for acceptable vibration levels in new helicopters, development of effective vibration reduction strategies has assumed greater importance in recent years. Fortunately, new active control strategies that are being considered have the potential for reducing vibration to levels that are substantially lower than what can be achieved using traditional passive approaches [1–3].

In forward flight, periodic aerodynamic loading on the blades is a major source of vibratory loads. Fairly mature active control strategies such as higher harmonic control (HHC) and individual blade control (IBC) attempt to modify these loads directly, at their source, by actively controlling the blade pitch at the root. The effectiveness of these approaches has been demonstrated in analytical simulations, wind tunnel tests, and flight tests. The levels of vibration reduction achieved vary between 70-90% [1]. However, there exist a number of problems associated with the practical implementation of these approaches in a production helicopter. These include high power consumption and airworthiness concerns arising from the need to modify the primary control system [1].

Recently, an alternative strategy for vibration reduction has emerged that is based on an actively controlled partial span trailing edge flap located at the outboard spanwise portion of the blade. Controlled deflection of this flap modifies the aerodynamic loading on the blade in a manner similar to HHC and IBC, without the need for oscillating the entire blade, or employing the primary control system for vibration reduction. Thus, the actively controlled trailing edge flap retains the most promising features of HHC and IBC while avoiding some of their disadvantages. Recent studies have confirmed these expectations and therefore improved analytical models are needed to enhance our understanding of this device and facilitate its development [1, 4–6].

A significant deficiency in existing analytical models is the lack of a suitable time domain unsteady aerodynamic theory to provide the sectional airloads needed to model the blade/actively controlled flap combination in compressible flow. Such a model has to be capable of representing (a) unsteady effects to accurately resolve the amplitude and phasing at high frequencies; (b) compressibility effects; (c) time varying freestream effects; and (d) unsteady control flap hinge moments. The model should also be computationally efficient.

A number of recent unsteady aerodynamic theories have been developed to model a airfoil/flap combination. Leishman and his associates [7–9] have developed a theory using an indicial approach that partially satisfies the above requirements. However, the hinge moment modeling capability is incomplete, and the model has not been extended to the time-varying freestream case (although a method has been suggested [10]). Another model has been developed by Peters and his co-workers [11]. However its details were presented for the incompressible case.

The principal objectives of this paper are: (1) To present a new compressible unsteady aerodynamic model, developed specifically for dynamic analysis of the blade/actively controlled flap combination, that meets the requirements stated above; (2) Validation of the new aerodynamic model; and (3) Implementation of the new aerodynamic model in an aeroelastic response analysis of a flexible hingeless blade, combined with a trailing edge flap.

Aerodynamic Modeling

A new two-dimensional unsteady aerodynamic model for an airfoil/trailing edge flap combination has been developed using an approach commonly employed in fixed wing aeroelastic applications [12–14]. In this approach, oscillatory aerodynamic response data is used to generate approximate transfer functions that relate airloads to generalized motions in the frequency domain. These expressions take the form of rational functions, which can be transformed to the time domain to yield a state space model for the aerodynamic loads that is compatible with control approaches and periodic systems.

In the present analysis, oscillatory lift, moment, and hinge moment response quantities for a two

dimensional flapped airfoil are generated using a doublet-lattice approach [15] based on the Possio integral equation [16]. Using this approach, oscillatory response quantities can be obtained for any airfoil/flap geometry at any reduced frequency and subsonic Mach number.

Airfoil motion is described by the generalized coordinates W_0 and W_1 which represent, respectively, airfoil motions producing constant and linearly varying normal velocity distributions on the airfoil as shown in Figure 1. These can be expressed in terms of the classical pitch and plunge coordinates α and h, shown in Figure 2, using the relations:

$$W_0(t) = U(t)\alpha(t) + \dot{h}(t), \tag{1}$$

$$W_1(t) = b\dot{\alpha}(t), \tag{2}$$

where, for simplicity, α and h are measured at the 1/4 chord of the airfoil. In a similar manner, flap motion is described by the generalized motions D_0 and D_1, which represent motions that produce constant and linearly varying normal velocity distributions on the flap, as shown in Figure 1. Using flap deflection δ and deflection rate $\dot{\delta}$, these can be written as

$$D_0(t) = U(t)\delta(t), \tag{3}$$

$$D_1(t) = b\dot{\delta}(t). \tag{4}$$

The normal velocity distributions associated with these generalized airfoil and flap motions are used by the doublet-lattice code to generate corresponding sets of oscillatory response data for each motion.

A convenient finite-dimensional approximation of the Laplace transformed unsteady airloads was developed by Roger [12]. The present study uses a variation of this approximation, given by

$$\mathrm{Q}(\tilde{p}) = C_0 + C_1\tilde{p} + \sum_{j=1}^{N_p} \frac{C_{j+1}\tilde{p}}{(\tilde{p}+\gamma_j)}, \tag{5}$$

where $\mathrm{Q}(\tilde{p})$ is a transfer function that relates generalized motion to an aerodynamic load. The coefficients C_n are chosen such that they provide a best fit, in a least squares sense, to oscillatory response data. The N_p terms in the series are aerodynamic lag terms, and contain an associated set of poles γ_j. The poles are assumed to be positive valued so as to produce stable open loop roots, but otherwise play a non-critical role in the approximation [12].

In general, the quality of the approximation depends on the number of lag terms N_p. However, when Eq. (5) is rewritten in state space form, each lag term will generate an aerodynamic state which is governed by a first order differential equation. In an aeroelastic simulation, aerodynamic state equations are coupled with the structural equations of motion, and must be solved simultaneously. Thus, the addition of lag terms to improve the accuracy of the approximation has to be balanced by the competing need for computational efficiency.

Using lift as an example, a frequency domain representation of the aerodynamic system can be written as

$$\mathcal{L}[C_l(s)U(s)] = \mathrm{C}_{\mathrm{l}_{\mathrm{W}_0}}(\tilde{p})\mathrm{W}_0(\tilde{p}) + \mathrm{C}_{\mathrm{l}_{\mathrm{W}_1}}(\tilde{p})\mathrm{W}_1(\tilde{p}), \tag{6}$$

where $\mathrm{W}_0(\tilde{p})$ and $\mathrm{W}_1(\tilde{p})$ represent Laplace transforms of $W_0(s)$ and $W_1(s)$ respectively. The transfer functions $\mathrm{C}_{\mathrm{l}_{\mathrm{W}_0}}(\tilde{p})$ and $\mathrm{C}_{\mathrm{l}_{\mathrm{W}_1}}(\tilde{p})$ are approximated by the following rational expressions, based on Eq. (5):

$$\mathrm{C}_{\mathrm{l}_{\mathrm{W}_0}}(\tilde{p}) = A_0 + A_1\tilde{p} + \sum_{j=1}^{N_{p1}} \frac{A_{j+1}\tilde{p}}{(\tilde{p}+\gamma_j)}, \tag{7}$$

$$\mathrm{C}_{\mathrm{l}_{\mathrm{W}_1}}(\tilde{p}) = B_0 + B_1\tilde{p} + \sum_{j=1}^{N_{p2}} \frac{B_{j+1}\tilde{p}}{(\tilde{p}+\kappa_j)}. \tag{8}$$

To identify the coefficients of the rational approximant, the nondimensional Laplace variable $\tilde{p}$ is first replaced by ik. Using Eq. (7) as an example, this yields

$$\mathrm{C}_{\mathrm{l}_{\mathrm{W}_0}}(k) = A_0 + A_1 ik + \sum_{j=1}^{N_{p1}} \frac{A_{j+1} ik}{(ik+\gamma_j)}. \tag{9}$$

A set of oscillatory response data is obtained, and can be written as

$$\mathrm{C}_{\mathrm{l}_{\mathrm{W}_0}}(k_n) = F(k_n) + iG(k_n), \quad n = 1 \ldots N_{dp}, \tag{10}$$

where N_{dp} is the number of reduced frequencies k_n for which response data has been generated. The approximants are constrained at $k = 0$ to recover the steady state response by setting

$$\mathrm{C}_{\mathrm{l}_{\mathrm{W}_0}}(0) = F(0) = A_0. \tag{11}$$

The remaining coefficients are identified using a least squares fit to the oscillatory response data. The approximant is then extended to the complex plane using analytical continuation.

Repeated Pole Formulation

A variety of different methods have been developed to reduce the number of lag terms (and resulting aerodynamic states) necessary to achieve a given level of accuracy [12, 14, 17]. The present model employs a simple variation on these approaches whereby the rational approximants associated with a particular aerodynamic load share a common set of poles. Using Eqs. (7) and (8) as an example, this yields

$$\mathrm{C}_{\mathrm{l}_{\mathrm{W}_0}}(\tilde{p}) = A_0 + A_1\tilde{p} + \sum_{j=1}^{N_p} \frac{A_{j+1}\tilde{p}}{(\tilde{p}+\gamma_j)}, \tag{12}$$

$$\mathrm{C}_{\mathrm{l}_{\mathrm{W}_1}}(\tilde{p}) = B_0 + B_1\tilde{p} + \sum_{j=1}^{N_p} \frac{B_{j+1}\tilde{p}}{(\tilde{p}+\gamma_j)}. \tag{13}$$

By repeating the poles, the total effective number of lag terms in this system is N_p instead of $2N_p$. This is evident by substituting Eqs.(12) and (13) into Eq. (6) to yield the single approximant

$$\mathcal{L}[C_l(s)U(s)] = (A_0+A_1\tilde{p})\mathrm{W}_0(\tilde{p})+(B_0+B_1\tilde{p})\mathrm{W}_1(\tilde{p}) + \sum_{j=1}^{N_p} \frac{(A_{j+1}\mathrm{W}_0(\tilde{p}) + B_{j+1}\mathrm{W}_1(\tilde{p}))\tilde{p}}{(\tilde{p}+\gamma_j)}, \quad (14)$$

with N_p lag terms. Note that when $N_p = N_{p2} + N_{p1}$, Eqs. (7) and (8) represent a special case of Eqs. (12) and (13). Thus, the repeated pole formulation imposes fewer restrictions on the choice of coefficients, and will generally produce a more accurate approximation. In practice, this means that a smaller number of lag terms is needed for a given level of accuracy, thus increasing the computational efficiency of the model.

Optimal Pole Placement

Pole placement is not critical to the approximation process, but can influence the fitting error. Numerical optimization techniques have been developed to find the pole locations that minimize this error [17–19]. In our case, this is accomplished using a standard numerical optimization routine. Casting the problem in the form:

$$\min_{\mathbf{x}_{dv}} F(\mathbf{x}_{dv}), \quad (15)$$

subject to the constraints

$$x_{Li} \le x_{dvi} \le x_{Ui}, \qquad i = 1 \ldots N_{dv}, \quad (16)$$

$$g_j(\mathbf{x}_{dv}) \le 0, \qquad j = 1 \ldots N_c, \quad (17)$$

where $\mathbf{x}_{dv}$ is a vector of N_{dv} design variables, $F(\mathbf{x}_{dv})$ is an objective function, and $g_j(\mathbf{x}_{dv})$ represents a set of constraint equations . In this case, the design variables are the poles γ_i, which are constrained only by the requirement that they be positive, and the objective function to be minimized is the least squares error parameter $\mathcal{X}^2$ which is used to fit the rational approximant to oscillatory response data.

In the repeated pole formulation, the choice of poles will effect the quality of fit in more than one approximation. This is a multiobjective optimization problem, and involves the selection of a 'best' design from a set of Pareto optimal solutions. This is carried out by creating a single objective function of the form

$$F(\mathbf{x}_{dv}) = \sum_{k=1}^{N_{of}} \lambda_k f_k(\mathbf{x}_{dv}), \quad (18)$$

using a set of N_{of} objective functions $f_k(\mathbf{x}_{dv})$, with λ_k taken to be scalar coefficients chosen such that

$$\sum_{k=1}^{N_{of}} \lambda_k = 1, \qquad \lambda_k \ge 0. \quad (19)$$

Using the lift expressions as an example, the approximants in Eqs. (12) and (13) will have the associated error parameters $\mathcal{X}^2_{W_0}$ and $\mathcal{X}^2_{W_1}$. Using Eqs. (18) and (19), these can be combined to yield a single objective function of the form

$$F(\mathbf{x}_{dv}) = \lambda\mathcal{X}^2_{W_0} + (1-\lambda)\mathcal{X}^2_{W_1}, \quad (20)$$

where $0 \le \lambda \le 1$. The optimization problem given in Eqs. (15)-(17) can then be restated as:

$$\min_{\gamma}(\lambda\mathcal{X}^2_{W_0} + (1-\lambda)\mathcal{X}^2_{W_1}), \quad (21)$$

subject to

$$\gamma_i \ge 0, \qquad i = 1 \ldots N_p. \quad (22)$$

Using this formulation, a standard numerical optimization code is used to generate optimal pole values for a given error weighting parameter λ.

State Space Model

To transform the rational approximant given in Eq. (14) to state space form, first define

$$\mathrm{X}_j(\tilde{p}) = \frac{(A_{j+1}\mathrm{W}_0(\tilde{p}) + B_{j+1}\mathrm{W}_1(\tilde{p}))\tilde{p}}{(\tilde{p}+\gamma_j)}, \quad (23)$$

where $j = 1 \ldots N_p$. Substituting Eq. (23) into Eq. (14), and taking the inverse Laplace transform yields the lift expression

$$C_l(s) = \frac{1}{U(s)}\left(A_0W_0(s) + A_1\frac{d}{ds}W_0(s) + B_0W_1(s) + B_1\frac{d}{ds}W_1(s) + \sum_{j=1}^{N_p} x_j(s)\right), \quad (24)$$

where the quantities x_j represent aerodynamic states. Taking the inverse Laplace transform of Eq. (23) yields the following set of first order differential equations governing the aerodynamic states:

$$\frac{d}{ds}x_j(s) + \gamma_j x_j(s) = A_{j+1}\frac{d}{ds}W_0(s) + B_{j+1}\frac{d}{ds}W_1(s), \quad (25)$$

where $j = 1 \ldots N_p$. Expressed in terms of time t, Eqs. (24) and (25) become

$$C_l(t) = \frac{1}{U(t)}\left(A_0W_0(t) + A_1\frac{b}{U(t)}\dot{W}_0(t) + B_0W_1(t) + B_1\frac{b}{U(t)}\dot{W}_1(t) + \sum_{j=1}^{N_p} x_j(t)\right), \quad (26)$$

$$\frac{b}{U(t)}\dot{x}_j(t) + \gamma_j x_j(t) = A_{j+1}\frac{b}{U(t)}W_0(t) + B_{j+1}\frac{b}{U(t)}W_1(t), \qquad j = 1 \ldots N_p. \quad (27)$$

The unsteady aerodynamic lift is given by Eq. (26), and is a function of the N_p aerodynamic states x_j. Each state is governed by a first order differential equation, given in Eq. (27), which is driven by the generalized airfoil motions.

Complete Sectional Aerodynamic Model

The complete RFA aerodynamic model for the airfoil and flap is composed of a set of constituent RFA aerodynamic components, which can be represented by

$$C_l = C_{l_A}(W_0, W_1) + C_{l_F}(D_0, D_1), \quad (28)$$

$$C_m = C_{m_A}(W_0, W_1) + C_{m_F}(D_0, D_1), \quad (29)$$

$$C_h = C_h(W_0, W_1, D_0, D_1), \quad (30)$$

where each term on the right side of Eqs. (28)-(30) represents an independent RFA component with an associated set of aerodynamic states and aerodynamic state equations. The subscripts A and F designate contributions due to airfoil motions and flap motions, which are modeled independently in Eqs. (28) and (29). This representation is convenient because it allows the model to be implemented at any point along a rotor blade, omitting the components associated with the flap at stations where they are not needed.

The component of the aerodynamic model providing the lift response to airfoil motions, represented by the term C_{l_A} in Eq. (28), is given in Eqs. (26) and (27). The remaining components of the model for lift and moment are obtained in an identical manner. Since these components have a form similar to that given in Eqs. (26) and (27), they will not be repeated here.

As indicated in Eq. (30), the contributions to hinge moment due to airfoil and flap motions are not modeled independently. In this case, a set of four rational approximants are used, each associated with a particular generalized airfoil or flap motion. These share a common set of N_{HP} poles, given by

$$C_{h_{W_0}}(\tilde{p}) = A_{H0} + A_{H1}\tilde{p} + \sum_{n=1}^{N_{HP}} \frac{A_{H(n+1)}\tilde{p}}{(\tilde{p} + \gamma_{Hn})}, \quad (31)$$

$$C_{h_{W_1}}(\tilde{p}) = B_{H0} + B_{H1}\tilde{p} + \sum_{n=1}^{N_{HP}} \frac{B_{H(n+1)}\tilde{p}}{(\tilde{p} + \gamma_{Hn})}, \quad (32)$$

$$C_{h_{D_0}}(\tilde{p}) = E_{H0} + E_{H1}\tilde{p} + \sum_{n=1}^{N_{HP}} \frac{E_{H(n+1)}\tilde{p}}{(\tilde{p} + \gamma_{Hn})}, \quad (33)$$

$$C_{h_{D_1}}(\tilde{p}) = F_{H0} + F_{H1}\tilde{p} + \sum_{n=1}^{N_{HP}} \frac{F_{H(n+1)}\tilde{p}}{(\tilde{p} + \gamma_{Hn})}. \quad (34)$$

The corresponding time-domain aerodynamic model for the hinge moment is given by

$$C_h(t) = \frac{1}{U(t)}\Big(A_{H0}W_0(t) + A_{H1}\frac{b}{U}\dot{W}_0(t) + B_{H0}W_1(t) + B_{H1}\frac{b}{U}\dot{W}_1(t) + E_{H0}D_0(t) + E_{H1}\frac{b}{U}\dot{D}_0(t) + F_{H0}D_1(t) + F_{H1}\frac{b}{U}\dot{D}_1(t) + \sum_{n=1}^{N_{HP}} z_n(t)\Big), \quad (35)$$

with the associated state equations

$$\frac{b}{U}\dot{z}_n(t) + \gamma_{Hn}z_n(t) = A_{H(n+1)}\frac{b}{U}\dot{W}_0(t) + B_{H(n+1)}\frac{b}{U}\dot{W}_1(t) + E_{H(n+1)}\frac{b}{U}\dot{D}_0(t) + F_{H(n+1)}\frac{b}{U}\dot{D}_1(t), \qquad n = 1 \ldots N_{HP}. \quad (36)$$

In the present analysis, the drag force is given by the static profile drag C_{do} of the airfoil section.

Structural Model

The hingeless rotor blade is modeled as a slender beam composed of a linearly elastic, homogeneous material, cantilevered at the hub as shown in Figure 3. The blade model is taken directly from Ref. 4 and describes the fully coupled flap-lag-torsional dynamics of an isotropic blade. Small strains and finite rotations (moderate deflections) are assumed, and the Bernoulli-Euler hypothesis is assumed to apply. In addition, strains within the cross-section are neglected. The equations of motion for the elastic blade consist of a set of nonlinear partial differential equations of motion, formulated in the undeformed system, with the distributed loads left in general symbolic form.

The control surfaces are assumed to be an integral part of the blade, attached at a number of spanwise locations using hinges that are rigid in all directions except about the hinge axis, constraining the control surface cross-section to pure rotation in the plane of the blade cross-section (see Fig. 3). The control surface does not provide a structural contribution to the blade, and influences the behavior of the blade only through its contribution to the blade spanwise aerodynamic and inertial loading.

In this study, the flap deflection is assumed to be a controlled quantity, and thus does not contribute an additional degree of freedom to the aeroelastic system.

Aeroelastic Formulation

Two approaches commonly used to formulate the aeroelastic equations of motion are the implicit approach and the explicit approach [20]. In the im-

plicit approach, the equations of motion do not appear as detailed expressions of the blade degrees of freedom, and are instead generated numerically, in matrix form, using a computer. The present analysis is based on an explicit approach, with the inertial, structural, damping, and aerodynamic terms appearing as explicit functions of the blade degrees of freedom and aerodynamic states. This approach allows term by term comparison of the equations of motion with models from other sources, adds physical insight, and is computationally efficient.

Explicit expressions for the distributed inertial, gravitational, and damping loads were derived in Ref. 4 using MACSYMA [26], and have been used in the present analysis. To keep these expressions of manageable size, an ordering scheme [21,22] was used based on a dimensionless parameter ϵ ($0.1 < \epsilon < 0.2$), which represents typical blade slopes due to elastic deformation. The ordering scheme implies that

$$1 + O(\epsilon^2) \approx 1, \tag{37}$$

so that terms of order $O(\epsilon^2)$ are neglected in comparison with unity.

Distributed Airloads

The formulation of distributed airloads is closely coupled with the method of solution. As part of the solution process, the aerodynamic loads must be evaluated at a number of specific spanwise locations along the blade span. The aerodynamic loads at these spanwise locations require a unique RFA aerodynamic model for each station.

One feature that complicates the RFA aerodynamic model when used in rotary wing aeroelastic applications is that the oscillatory response data must be generated for a specific value of Mach number. However, the velocity distribution along the span of a rotor blade changes as a function of azimuth due to forward flight and also due to blade dynamics in the chordwise direction.

Two corrections to the RFA aerodynamic model were developed to take into account the spanwise and azimuthal variation of the Mach number. The first correction was implemented as follows: The rotor disk was divided into a number of azimuthal segments. Neglecting the contribution of the blade flexibility, the velocity in the plane of the disk depends only on the azimuth and the radial location along the blade span. Using this velocity allows one to define a constant Mach number within the azimuthal segment by taking the average of the Mach numbers at the region boundaries. Using this Mach number, an RFA aerodynamic model is constructed for the azimuthal segment. This is repeated for a desired number of azimuthal segments, producing a varying RFA aerodynamic model around the rotor disk. The transition of the blade from one segment to another requires only a change in the coefficients of the aerodynamic model (i.e. the coefficients A_j and B_j in Eqs. (26) and (27)). However, this introduces an undesirable discontinuity in the aerodynamic loads.

This problem is remedied by recognizing that, in the limit, as the number of azimuthal segments becomes infinite, the coefficients of the RFA aerodynamic model will change continuously as functions of ψ. The Mach number is also an explicit function of ψ when blade dynamics are neglected. Using coefficients of the RFA model generated at various values of Mach number, the dependence of each coefficient on M can be represented by an approximate function generated using a least squares fit. Using this approach, a new correction is implemented as follows: The velocity in the plane of the disk is evaluated for a given blade station over one revolution to determine the upper and lower bounds on the Mach number. A set of Mach numbers are then selected that span this Mach number range in increments of 0.02. At each of these Mach numbers, an RFA aerodynamic model is generated. The coefficients of each aerodynamic model are thus known at intervals of Mach number, and constitute data points that can be used to develop approximate expressions for each coefficient, as a function of Mach number, using a least squares fit. These approximate coefficient functions are then used to replace the original coefficients in the sectional aerodynamic model. Poles are taken to be constant at each blade station, and are optimized at the beginning of the process to produce a minimum error approximant at the mean Mach number.

Method of Solution

The solution of the rotary-wing aeroelastic response problem is carried out in two steps. First, spatial discretization based on Galerkin's method [21] is used to eliminate the spatial dependence, and subsequently the combined structural and aerodynamic state equations are solved in the time domain.

In this study, Galerkin's method is based on three flap, two lead-lag, and two torsional free vibration modes of a rotating beam. The free vibration modes were calculated using the first nine exact nonrotating modes of a uniform cantilevered beam. Integrations over the blade span associated with the application of Galerkin's method are carried out using Gaussian quadrature. This requires that the integrand be evaluated at a fixed number of stations along the span of the blade corresponding to Gaussian points which are determined by the order of Gaussian quadrature being used. The number and location of these stations must be carefully combined with the implementation of the RFA aerodynamic model. At each station, the sectional airloads are provided by a specific RFA aerodynamic approximation, each contributing a number of aerodynamic state equations to the final model. These state equations are fully coupled with

the blade equations of motion through the blade degrees of freedom and aerodynamic states.

The complete aeroelastic model for the blade and actively controlled flap consists of three sets of equations. The first two sets consist of nonlinear differential equations that describe the structural degrees of freedom and aerodynamic states. The equations of motion for the elastic blade are represented by the expression

$$\mathbf{f_b}(\mathbf{q_b}, \dot{\mathbf{q}}_\mathbf{b}, \ddot{\mathbf{q}}_\mathbf{b}, \mathbf{x_a}, \mathbf{q_t}; \psi) = \mathbf{0}, \tag{38}$$

where $\mathbf{q_b}$ represents the vector of blade degrees of freedom, $\mathbf{x_a}$ represents the vector of aerodynamic states, and $\mathbf{q_t}$ represents the trim vector, given by

$$\mathbf{q_t} = \{\lambda, \alpha_R, \theta_0, \theta_{1c}, \theta_{1s}\}^T, \tag{39}$$

where λ is the inflow ratio, α_R is the rotor pitch angle, and θ_0, θ_{1c}, and θ_{1s} are the collective and cyclic pitch inputs. Similarly, the complete set of aerodynamic state equations are represented by the expression

$$\mathbf{f_a}(\mathbf{q_b}, \dot{\mathbf{q}}_\mathbf{b}, \ddot{\mathbf{q}}_\mathbf{b}, \mathbf{x_a}, \dot{\mathbf{x}}_\mathbf{a}, \mathbf{q_t}; \psi) = \mathbf{0}, \tag{40}$$

A third set of equations are used to represent a propulsive trim condition in which force equilibrium is enforced in the vertical plane, and pitch and roll moments are set equal to zero. These equations were derived in Ref. 4 and include an inflow equation. They can be symbolically represented by the expression

$$\mathbf{f_t}(\mathbf{q_b}, \dot{\mathbf{q}}_\mathbf{b}, \ddot{\mathbf{q}}_\mathbf{b}, \mathbf{x_a}, \mathbf{q_t}; \psi) = \mathbf{0}. \tag{41}$$

To obtain the coupled trim/response solution, only the steady state response of the system is considered. In this case, the trim condition can be represented by the implicit nonlinear equations

$$\mathbf{f_t}(\mathbf{q_t}) = \mathbf{0}. \tag{42}$$

Evaluation of Eqs. (42) requires the steady state hub loads that correspond to the trim parameters $\mathbf{q_t}$. These are obtained by integrating Eqs. (38) and (40) numerically over time, until the response solution has converged to the steady state.

The trim solution $\mathbf{q_t}$ is currently obtained using a simple discrete time controller. This control strategy is based on the minimization of a performance index that is a quadratic function of the trim residuals $\mathbf{R_i}$, where

$$\mathbf{f_t}(\mathbf{q}_{t_i}) = \mathbf{R_i}, \tag{43}$$

at the ith time step. An optimal controller is obtained using a linear, quasistatic representation of the response to control $\mathbf{q_t}$, given by

$$\mathbf{R_i} = \mathbf{R}_{i-1} + [T_o](\mathbf{q}_{t_i} - \mathbf{q}_{t_{i-1}}), \tag{44}$$

where $[T_o]$ is a matrix of control sensitivities given by

$$[T_o] = \frac{\partial \mathbf{R}}{\partial \mathbf{q_t}}, \tag{45}$$

evaluated about the set of initial trim parameters $\mathbf{q}_{t_0}$.

Results and Discussion

The sectional RFA aerodynamic model for the airfoil/flap combination uses twelve separate rational approximations to represent the transfer functions relating lift, moment, and hinge moment to each of four generalized airfoil and flap motions. The process of fitting these approximants to oscillatory response data involves five separate pole optimizations, one for each aerodynamic component shown in Eqs. (28)-(30). Figures 5 through 7 present typical examples of optimized rational approximations that are used in the sectional aerodynamic model for the airfoil/flap combination. The figures show the lift, moment, and hinge moment response to oscillatory D_0 motion, approximated using one, two, and three lag term rational approximants. The oscillatory response data used to derive these approximants was generated using the doublet-lattice approach at $M = 0.7$ and a reduced frequency range 0.0-0.4.

Figure 5 shows that the accuracy of the lift response to D_0 motion improves with each additional lag term. For this case, the approximation based on two lag terms seems to be more accurate than the single lag approximation. However, the difference between the two and three lag approximations is small, and both exhibit good agreement with the doublet-lattice data points. This suggests that, in this case, the addition of a third lag term may not be cost effective.

The moment response to D_0 motion, shown in Fig. 6, exhibits similar characteristics to those evident in the lift plot. In this case, the approximation based on two lag terms is again superior to the single lag approximation, and the responses corresponding to the two and three lag term approximations are almost identical, displaying close agreement to the doublet-lattice data points. Again, the improvement in accuracy due to the addition of a third lag term does not appear to justify the additional aerodynamic state.

For the hinge moment response to D_0 motion, shown in Fig. 7, the approximations based on one and two lag terms are very similar and the best agreement with doublet-lattice data is obtained when using three lag terms.

The approximations generated for the remaining generalized airfoil and flap motions are not substantially different from those presented in Figs. 5-7. These results provide insight into the state variable requirements of the RFA aerodynamic model. For the case presented here, two lag terms appear to provide sufficient accuracy for each of the four lift and moment components given in Eqs. (28) and (29). Assuming three lag terms for the hinge moment model, Eq. (30), a total of eleven states would be necessary to completely model the compressible unsteady lift, moment, and hinge moment of a flapped airfoil section. However, actual state variable requirements

could be higher or lower, depending upon the application. The differences in modeling accuracy are somewhat exaggerated by the scale used in the plots in Figs. 5 through 7, and a single lag term could probably be sufficient for many applications thereby reducing the number of aerodynamic states needed. Alternatively, it may be necessary to fit the approximants to oscillatory data taken over a wider range of reduced frequencies, particularly if high frequency flap motion is required. For such situations, the number of lag terms required for a certain level of accuracy could increase, requiring a larger number of aerodynamic states for time domain modeling.

Another aspect of the RFA aerodynamic model that needed to be validated was its behavior in an oscillating freestream. For this purpose, results from our model were compared with an exact incompressible solution to the time varying freestream problem obtained by Isaacs [24], and later extended in Ref. 25 to account for plunge motion and pitch variation about an arbitrary axis. The manner in which this comparison was conducted is similar to that used in Ref. 10. Only unsteady lift is considered, and the freestream velocity was assumed to be represented by

$$U(t) = U_o \left[1 + \lambda_u \sin\psi\right]. \qquad (46)$$

The reduced frequency of oscillation is 0.2, and $\lambda_u = 0.8$ representing large amplitude freestream velocity variations. Unsteady lift results were generated for three types of pitch motion: $\alpha = \alpha_o$ (constant), $\alpha = \sin\psi$, and $\alpha = \cos\psi$, with lift normalized by the static value at constant angle of attack given by $C_{l_o} = 2\pi\alpha_o$. Results are shown in Figures 8 through 10 for the incompressible case. Results were generated for the RFA aerodynamic model using approximations based on one and two lag terms, each fitted to oscillatory data taken over a reduced frequency range of 0.0-0.8.

For the case of constant angle of attack, Fig. 8, excellent agreement between the response of the RFA aerodynamic model and the exact theory [24] is evident. There is no visible difference between the responses from the one and two lag term approximations. For angle of attack varying with $\sin\psi$, shown in Fig. 9, good agreement between the response of the RFA aerodynamic model and the exact theory [24] is again evident. In this case, the approximation based on two lag terms is slightly more accurate than that based on a single lag term. Similar results are presented in Fig. 10 for the case when angle of attack varies as $\cos\psi$.

Next, a few preliminary results are presented showing the blade aeroelastic response behavior with the RFA aerodynamics incorporated in the rotor aeroelastic analysis. Figures 11 and 12 show, respectively, the aerodynamic lift and moment distributions on an isolated blade, over one revolution, for a trimmed rotor at an advance ratio of 0.4. A soft-in-plane blade configuration was used, given in Table 1. The quantities X_{FA}, Z_{FA}, X_{FC}, Z_{FC} represent offsets of the helicopter aerodynamic center and center of gravity, as shown in Figure 4. All parameters have been nondimensionalized using the unit quantities

[length]	=	R,	rotor radius,
[mass]	=	M_b,	mass of one blade,
[time]	=	$\frac{1}{\Omega}$,	inverse of the rotor speed.

where $R = 4.91$ m, $M_b = 52$ kg, and $\Omega = 425$ RPM, similar to a MBB-105 helicopter [28]. Lift and moment have been nondimensionalized by dividing by the quantities $M_b\Omega^2 R$ and $M_b\Omega^2 R^2$, respectively. The upper plot in both figures presents the response obtained using the new RFA aerodynamic model with two lag terms, and the lower plot presents the response obtained using the modified quasisteady incompressible Theodorsen aerodynamics described in Ref. 4. The configuration of the RFA aerodynamic model is summarized in Table 2. For this comparison, the quasisteady Theodorsen results were found using the same blade response solution that was generated using the RFA aerodynamic model. It was assumed that by using the same blade motion, differences in the the loading distributions would better reflect differences in the aerodynamic models.

Significant differences in the amplitude and phasing of the aerodynamic loads predicted by the two models is evident in both figures, particularly in the outer region of the blade where compressibility effects are most pronounced. In Fig. 11, the largest differences in the predicted lift distributions occur on the advancing side, $0 < \psi < \pi$. In this region, the lift predicted by the RFA aerodynamic model at the end of the blade is approximately 50% greater than that predicted by the quasisteady Theodorsen model, with a smaller phase shift. A similar behavior can be seen in the moment distribution shown in Fig. 12. On the advancing side, the RFA aerodynamic model predicts moments that are approximately three times greater at the tip of the blade than those predicted using quasisteady aerodynamics. In vibration reduction studies using the actively controlled trailing edge flap [4], the flap was usually centered at 75% of the blade span. Thus, the results shown in Figs. 11 and 12 reaffirm the need for a compressible flow, unsteady aerodynamic model for analysis of the actively controlled trailing edge flap.

Concluding Remarks

Recent studies of the actively controlled trailing edge flap have revealed a need for improved aerodynamic models for the blade/flap combination. To address this need, a new two dimensional unsteady aerodynamic model for an airfoil/flap combination has been developed that includes the effects of compressibility and time-varying oncoming flow velocity.

The model is expressed in state space form, and results indicate that only a small number of states are required for aerodynamic modeling. Thus, the model is efficient, and suitable for vibration reduction studies using trailing edge flaps.

The results show that in many cases, a good approximation for the time domain aerodynamics can be obtained using only a few aerodynamic states. Preliminary results for blade response reinforce the need for time domain compressible modeling when calculating the loads in the flap region.

Acknowledgments

This work was supported partially by the NASA Graduate Student Researchers Program NASA NGT-51173, and in part by Army Grant DAAH04-95-1-0095 funded by the Army Research Office.

References

[1] Friedmann, P.P., and Millott, T.A., "Vibration Reduction in Rotorcraft Using Active Control: A Comparison of Various Approaches," *Journal of Guidance, Control, and Dynamics*, Vol. 18, No. 4, July-August 1995, pp. 664-673.

[2] Loewy, R.G., "Helicopter Vibrations, A Technological Perspective," *AHS Journal*, Vol. 29, October 1984, pp. 4-30.

[3] Reichert, G., "Helicopter Vibration Control: A Survey," *Vertica*, Vol. 5, No. 7, 1981, pp. 1-20.

[4] Millott, T.A., and Friedmann, P.P., "Vibration Reduction in Hingeless Rotors using an Actively Controlled Partial Span Trailing Edge Flap Located on the Blade," NASA CR-4611, June 1994.

[5] Straub, F.K., "Active Flap Control for Vibration Reduction and Performance Improvement," Proceedings of the 51st American Helicopter Society Forum, Fort Worth, TX, 1995, pp. 381-392.

[6] Milgram, J., and Chopra, I., "Helicopter Vibration Reduction With Trailing Edge Flaps," AIAA Paper 95-1227-CP, Proceedings of the 36th AIAA/ASME/ASCE/AHS/ASC Structures, Structural Dynamics and Materials Conference, New Orleans, LA, April 10-12, 1995, pp. 601-612.

[7] Leishman, J.G., and Nguyen, K.Q., "A State-Space Representation of Unsteady Aerodynamic Behavior," *AIAA Journal*, Vol. 28, No. 5, May 1990, pp. 836-845.

[8] Leishman, J.G., "Unsteady Lift of a Flapped Airfoil by Indicial Concepts," *Journal of Aircraft*, Vol. 31, No. 2, March-April 1994, pp. 288-297.

[9] Hariharan, N., and Leishman, J.G., "Unsteady Aerodynamics of a Flapped Airfoil in Subsonic Flow by Indicial Concepts," AIAA Paper 95-1228-CP, Proceedings of the 36th AIAA/ASME/ASCE/AHS/ASC Structures, Structural Dynamics and Materials Conference, April 10-12, 1995, New Orleans, LA, pp. 613-634.

[10] van der Wall, B.G., and Leishman, J.G., "On the Influence of Time-Varying Flow Velocity on Unsteady Aerodynamics," *Journal of the American Helicopter Society*, October 1994, pp. 25-36.

[11] Peters, D.A., and Johnson, M.J., "Finite-State Airloads For Deformable Airfoils on Fixed and Rotating Wings," *Aeroelasticity and Fluid Structure Interaction Problems*, Proceedings of the ASME Winter Annual Meeting, Chicago, November 6-11, 1994, AD-Vol. 44, pp. 1-28.

[12] Roger, K.L., "Airplane Math Modeling Methods for Active Control Design," Structural Aspects of Active Controls, AGARD-CP-228, Aug. 1977, pp. 4.1-4.11.

[13] Edwards, J.H., Ashley, H., and Breakwell, J., "Unsteady Aerodynamic Modeling for Arbitrary Motion," *AIAA Journal*, Vol. 17, No. 4, April 1979, pp. 365-374.

[14] Vepa, R., "Finite State Modeling of Aeroelastic Systems," NASA CR-2779, 1977.

[15] Albano, E., and Rodden, W.P., "A Doublet-Lattice Method for Calculating Lift Distributions on Oscillating Surfaces in Subsonic Flows," *AIAA Journal*, Vol. 7, No. 2, February 1969, pp. 279-285.

[16] Possio, C., "L'Azione Aerodinamica sul Profilo Oscillante in un Fluido Compressibile a Velocita Iposonora," *L' Aerotecnica*, t. XVIII, fasc. 4, April 1938. (Also available as British Ministry of Aircraft Production R.T.P translation 987)

[17] Karpel, M., "Design for Active and Passive Flutter Suppression and Gust Alleviation," NASA CR-3482, 1981.

[18] Sherwood, T.H., and Adams, W.M., "Nonlinear Programming Extensions to Rational Function Approximation Methods for Unsteady Aerodynamic Forces," NASA TP-2776, 1988.

[19] Peterson, L.D., and Crawley, E.F., "Improved Exponential Time Series Approximations of Unsteady Aerodynamic Operators," *Journal of Aircraft*, Vol. 25, No. 2, 1988, pp. 121-127.

[20] Friedmann, P.P., and Hodges, D.H., "Rotary-Wing Aeroelasticity with Application to VTOL Vehicles," *Flight-Vehicle Materials, Structures,*

and Dynamics- Assessment and Future Direction, Vol. 5, Structural Dynamics and Aeroelasticity, (Edited by A.K. Noor and S.L. Venneri), published by ASME 1993, Chapter 6, pp. 299-391.

[21] Friedmann, P.P., "Formulation and Solution of Rotary-Wing Aeroelastic Stability and Response Problems," *Vertica*, Vol. 7, No. 2, 1983, pp. 101-141.

[22] Crespo Da Silva, M.R.M, and Hodges, D.H., "The Role of Computerized Symbolic manipulations in Rotorcraft Dynamic Analysis," *Computer and Mathematics with Application*, Vol. 12A, 1986, pp. 161-172.

[23] Shampine, L.F, and Gordon, M.K., *Computer Solution of Ordinary Differential Equations- The Initial Value Problem*, W.H. Freeman and Co., San Francisco, CA, 1975.

[24] Isaacs, R., "Airfoil Theory for Rotary Wing Aircraft," *Journal of the Aeronautical Sciences*, Vol. 13, No. 4, pp. 218-220.

[25] van der Wall, B., "The Influence of Variable Flow Velocity on Unsteady Airfoil Behavior," UMAREO 91-46, M.S. Thesis, University of Maryland, College Park, 1991. Also available as DLR-FB 92-22.

[26] _____, "MACSYMA: Mathematics and System Reference Manual," 15th Edition, 1995.

[27] Millott, T.A., and Friedmann, P.P., "Vibration Reduction in Hingeless Rotors Using an Actively Controlled Trailing Edge Flap: Implementation and Time Domain Simulation," AIAA Paper 94-1306-CP, Proceedings of the 35th AIAA/ASME/ASCE/AHS/ASC 35th Structures, Structural Dynamics, and Materials Conference, Hilton Head, SC, April 18-20, 1994, pp. 8-22.

[28] Staley, J.A., "Validation of Rotorcraft Flight Simulation Program Through Correlation with Flight Data for Soft-in-Plane Hingeless Rotors," USAAMRDL-TR-75-50, January 1976.

Table 1: Soft-in-plane elastic blade configuration

Rotor Data	
$N_b = 4$	$L_b = 1.0$
$c_b = 0.05498$	$\theta_{pt} = 0$
$\omega_F = 1.123, 3.41, 7.65$	$C_{do} = 0.01$
$\omega_L = 0.732, 4.485$	
$\omega_{T1} = 3.17$	
$\gamma = 5.5$	$\sigma = 0.07$
Helicopter Data	
$C_W = 0.005$	$fC_{df} = 0.01A_R$
$X_{FA} = 0.0$	$Z_{FA} = 0.25$
$X_{FC} = 0.0$	$Z_{FC} = 0.5$

Table 2: RFA aerodynamic model parameters

Number of lag terms:	2 Lag Terms, Lift
	2 Lag Terms, Mom.
Reduced Freq. Range:	0.0-0.4
# of Blade Stations:	10
Total Aerodynamic States:	40

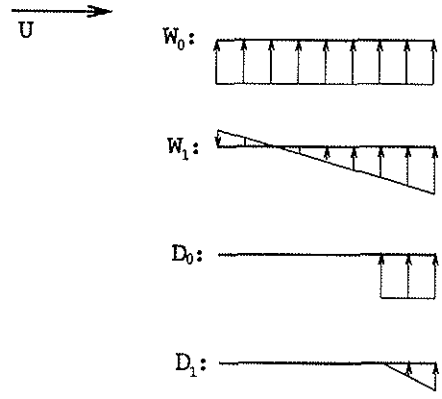

Figure 1: Normal velocity distributions corresponding to generalized airfoil and flap motions W_0, W_1, D_0, and D_1.

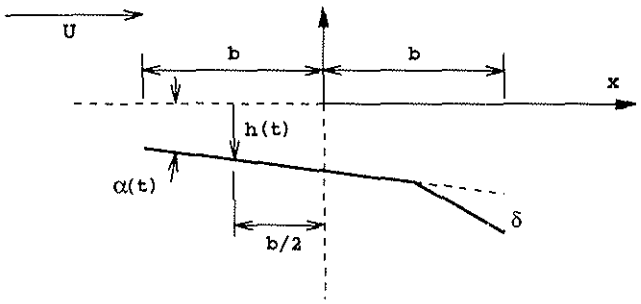

Figure 2: Airfoil/flap combination undergoing pitching and plunging motions.

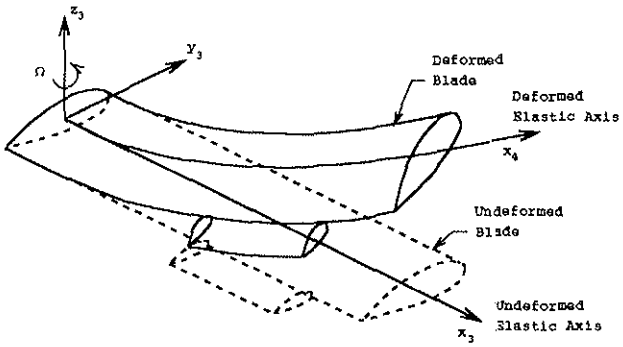

Figure 3: Fully elastic blade model incorporating a partial span trailing edge flap.

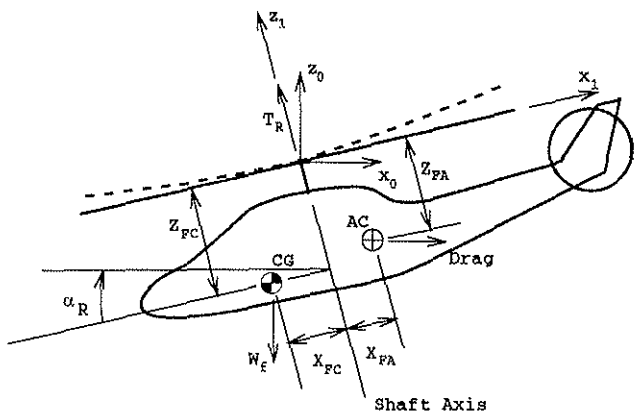

Figure 4: Schematic of a helicopter in level forward flight.

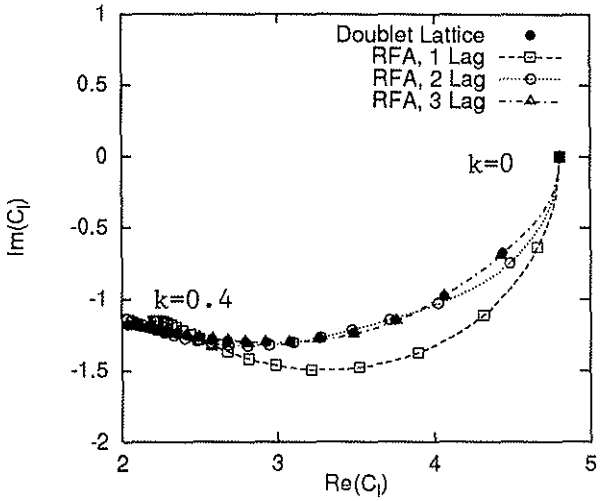

Figure 5: Rational function approximation of the C_l response to oscillatory D_0 motion at $M = 0.7$, over reduced frequency range $k = 0.0 - 0.4$, using 1, 2, and 3 lag term approximants.

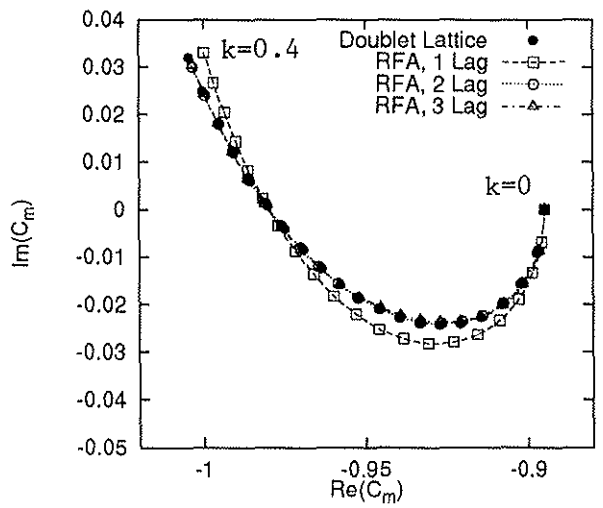

Figure 6: Rational function approximation of the C_m response to oscillatory D_0 motion at $M = 0.7$, over reduced frequency range $k = 0.0 - 0.4$, using 1, 2, and 3 lag term approximants.

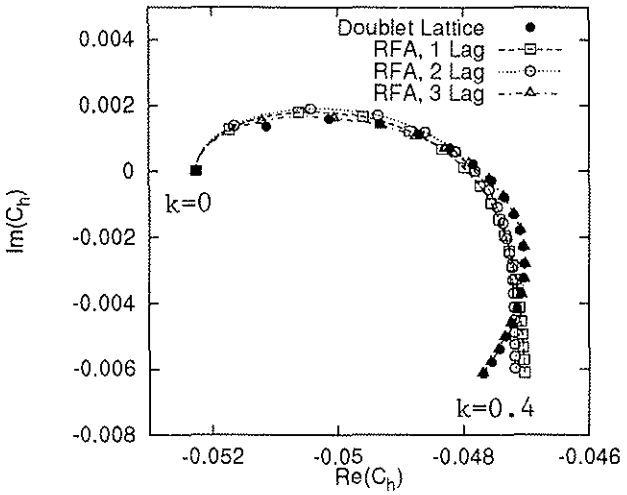

Figure 7: Rational function approximation of the C_h response to oscillatory D_0 motion at $M = 0.7$, over reduced frequency range $k = 0.0 - 0.4$, using 1, 2, and 3 lag term approximants.

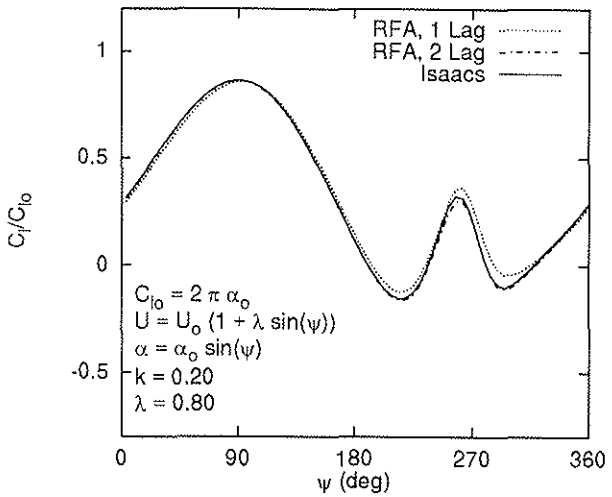

Figure 9: C_l response to freestream velocity variation, angle of attack varying with $\sin(\psi)$, $M = 0$.

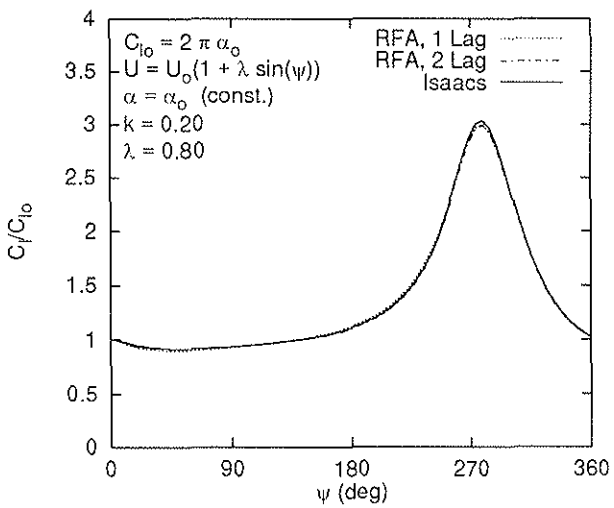

Figure 8: C_l response to freestream velocity variation with constant angle of attack, $M = 0$.

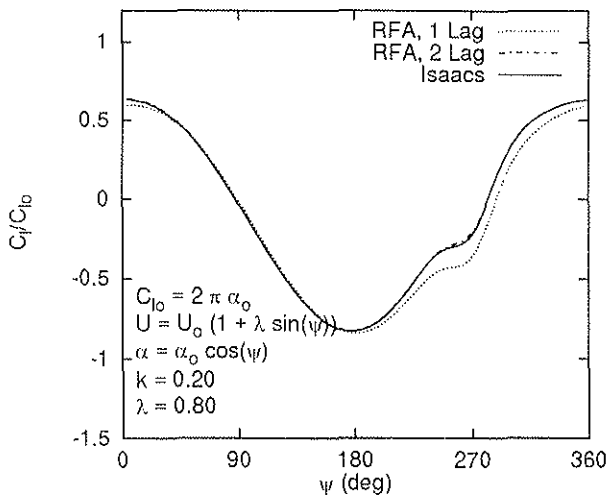

Figure 10: C_l response to freestream velocity variation, angle of attack varying with $\cos(\psi)$, $M = 0$.

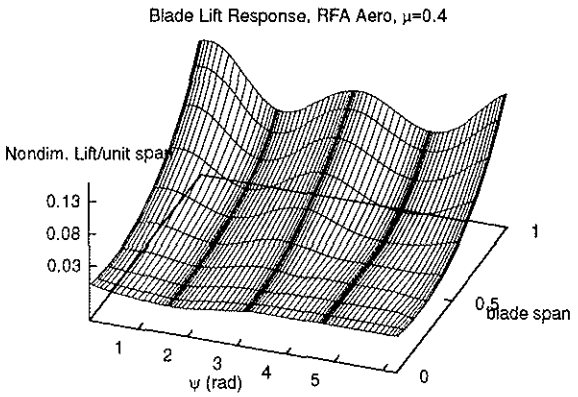

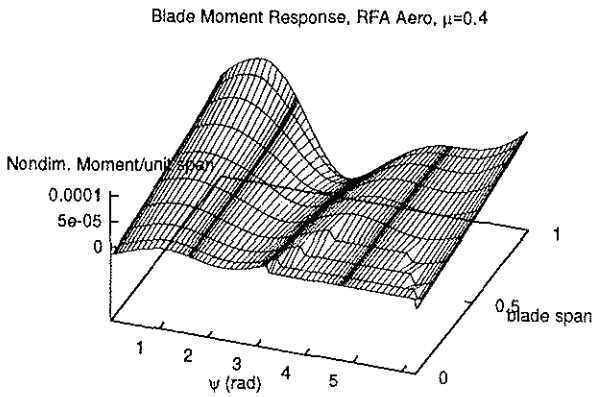

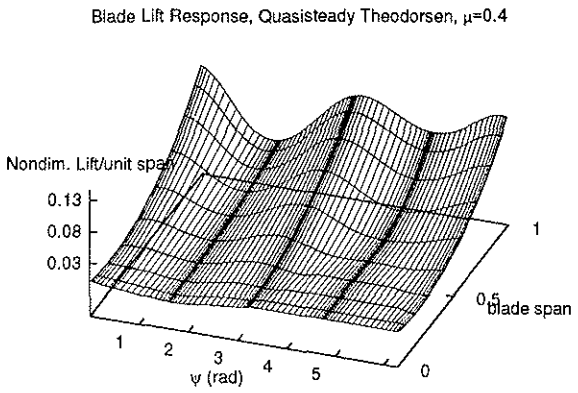

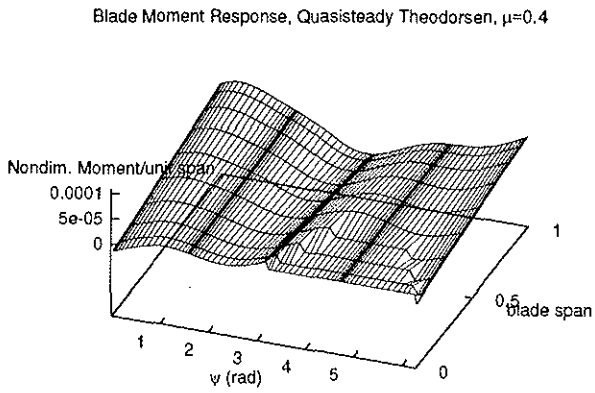

Figure 11: Blade lift distribution over one revolution, $\mu = 0.4$, using RFA aerodynamic model (upper plot) and quasisteady Theodorsen aerodynamics (lower plot).

Figure 12: Blade lift distribution over one revolution, $\mu = 0.4$, using RFA aerodynamic model (upper plot) and quasisteady Theodorsen aerodynamics (lower plot).